

---

# Reliability of signal transmission in stochastic nerve axon equations

Martin Sauer · Wilhelm Stannat

February 13, 2015

**Abstract** We introduce a method for computing probabilities for spontaneous activity and propagation failure of the action potential in spatially extended, conductance-based neuronal models subject to channel noise, based on statistical properties of the membrane potential. We compare different estimators with respect to the quality of detection, computational costs and robustness and propose the integral of the membrane potential along the axon as an appropriate estimator to detect both spontaneous activity and propagation failure. Performing a model reduction we achieve a simplified analytical expression based on the linearization at the resting potential (resp. the traveling action potential). This allows to approximate the probabilities for spontaneous activity and propagation failure in terms of (classical) hitting probabilities of one-dimensional linear stochastic differential equations. The quality of the approximation with respect to the noise amplitude is discussed and illustrated with numerical results for the spatially extended Hodgkin-Huxley and the simpler FitzHugh-Nagumo model.

**Keywords** Stochastic spatial model neuron · Hodgkin-Huxley equations · FitzHugh-Nagumo equations

## 1 Introduction

Noise is an inherent component of neural systems that accounts for various problems in information processing

---

This work is supported by the BMBF, FKZ 01GQ1001B.

M. Sauer (✉), W. Stannat  
Institut für Mathematik, Technische Universität Berlin,  
Straße des 17. Juni 136, D-10623 Berlin, Germany and  
Bernstein Center for Computational Neuroscience,  
Philippstr. 13, D-10115 Berlin, Germany.  
E-mail: sauer@math.tu-berlin.de

at all levels of the nervous system, see e. g. the review Faisal et al. (2008) for a detailed discussion. In particular, channel noise has been identified as an important source of various types of variability in single neurons. Exemplarily, we think of noise induced phenomena as observed in Faisal & Laughlin (2007). The timing of action potentials can be highly sensitive with respect to fluctuations in the opening and closing of ion channels leading to jitter and stochastic interspike intervals (Horikawa, 1991). This effect becomes important in thin axons with diameter of less than  $1\mu\text{m}$ . Furthermore, there appear stochastic patterns in the grouping of action potentials, and action potentials can vanish due to noise interference or spontaneously emerge without apparent synaptic input.

When it comes to the mathematical modeling of the membrane potential in axons, in particular in thin ones, channel noise therefore has to be taken into account. For a discussion and comparison of the various types of adding noise to conductance-based neuronal models such as the classical Hodgkin-Huxley equations we refer to Goldwyn & Shea-Brown (2011). Concerning spatially extended models, in e. g. Tuckwell & Jost (2010, 2011); Tuckwell (2008) it has been shown that already simple additive noise, uncorrelated in space and time, accounts for a large range of variability in the action potential. That includes variability in the repetitive generation of action potentials, deletion of action potentials or *propagation failures* and spontaneously emerging action potentials or *spontaneous activity*.

It is the purpose of this work to introduce a method to compute in a mathematical consistent way the probabilities of those last two events. This is done for general spatially extended neuronal models with additive noise, both numerically and theoretically, in terms of statistical quantities of the membrane potential. A suit-

able statistical estimator for such kind of characteristics should have the following desired properties: It is automatically evaluable to do Monte-Carlo simulations; it strictly separates the considered event from different ones; it is a low dimensional function of the observables; it is relatively robust to stochastic perturbations and uncertainty in the observables. We compare different estimators with respect to the quality of detection, computational costs and robustness. In order to further reduce the computational costs and to obtain a simpler analytical description, we perform a consistent model reduction, with respect to these statistical quantities, to a one-dimensional linear stochastic differential equation that allows to compute the desired characteristics without necessarily simulating the full system.

The method is illustrated in a case study using the Hodgkin-Huxley equations (Hodgkin & Huxley, 1952) and the more theoretical FitzHugh-Nagumo equations (FitzHugh, 1969). Both systems of partial differential equations can serve as a model for the propagation of action potentials in the neuron's axon. In particular, depending on the size of the stimulus there exist pulse-like solutions (action potentials) to these equations propagating along the spatial domain. Using these equations, we estimate the probabilities of *spontaneous activity* and *propagation failure*. Although we only focus on these two examples, the methods presented here can be used for a broader range of problems, in particular, similar model reductions can also be performed in order to compute time jitter and the variability in grouping patterns of action potentials.

In our setting, we consider both FitzHugh-Nagumo and Hodgkin-Huxley equations with a simple spatial geometry of the axon that is a cylindrical shaped fiber. Thus the relevant spatial domain is a interval  $[0, L]$ . We propose  $\Phi(u) := \int_0^L u(x) dx$  as an estimator for the detection of spontaneous activity and propagation failures. Here,  $u$  is the space(-time)-dependent observable whose solution is pulse-formed. In the cases at hand, this will be the membrane potential.  $\Phi(u)$  is the area under the pulse considered as a graph with respect to the space variable that has the following properties: It is easy to extract automatically from the numerical simulations; it significantly separates the number of observed pulses; it is a linear functional of only one observable; stochastic perturbations, in particular additive noise that is white in space (or of low correlation length) should cancel out through integration. The events of *spontaneous activity* and *propagation failure* can both be defined as threshold crossings of the quantity  $\Phi(u)$  and therefore easily be estimated using a Monte-Carlo simulation. The results can be found in Sections 3 and 4. In Section 5, we do a model reduc-

tion for this quantity, only assuming a reasonable local stability of the pulse and resting solutions. In particular, we deduce one-dimensional Ornstein-Uhlenbeck processes, that captures both probabilities reasonably well.

## 2 The mathematical model

In this article, we consider spatially extended conductance based neuronal models with a simple one dimensional domain  $(0, L)$  approximating the axon. This is most accurate in the case of a long axon, shaped as a cylinder with constant diameter. All examples are realized as a stochastic partial differential equation (SPDE) on the Hilbert space  $(H, \|\cdot\|) = L^2(0, L)$  with inner product  $\langle \cdot, \cdot \rangle$ . For the spatial diffusion, define the Laplace operator  $\Delta u := \partial_x^2 u$ ,  $u \in W^{2,2}(0, L)$ , supplemented with Neumann boundary conditions. We choose a sealed end at  $x = L$ , i. e.  $\partial_x u(t, L) = 0$  for all  $t \geq 0$  and model the input signal to the axon via an injected current in form of a rectangular pulse

$$\partial_x u(t, 0) = J(t), \quad J(t) = \mathbb{1}_{[0, T^*]}(t)J. \quad (1)$$

Here,  $T^* \leq \infty$  is the duration and  $J > 0$  the amplitude of the signal,  $\mathbb{1}$  stands for the indicator function.

The driving noise is a two-parameter white noise defined in terms of a cylindrical Wiener process  $W(t)$  that can be formally represented by the infinite series

$$W(t, x) := \sum_{n=1}^{\infty} e_n(x)\beta_n(t),$$

where  $(\beta_n(t))_{n \in \mathbb{N}}$  is a family of iid real valued Brownian motions and

$$e_n(x) := \sqrt{\frac{2}{L}} \cos\left(2\pi \frac{k}{L}x\right)$$

is an orthonormal basis of  $H$ . For  $f, g \in H$  one can calculate the covariance of this process as

$$\mathbb{E}[\langle W(t), f \rangle \langle W(s), g \rangle] = (t \wedge s) \langle f, g \rangle,$$

thus no correlation in either time nor space.

Together with suitable initial conditions we refer to Sauer & Stannat (2015, 2014) for well-posedness of such equations, in particular, the FitzHugh-Nagumo and the Hodgkin-Huxley equations.

## 2.1 FitzHugh-Nagumo equations

The FitzHugh-Nagumo (FHN) equations, in our case involving spatial diffusion, have been initially obtained as a mathematical simplification of the more complex Hodgkin-Huxley equations by Nagumo et al. (1962); FitzHugh (1961, 1969). They describe the evolution of the membrane potential  $u(t, x)$  in time and space, together with a recovery variable  $v(t, x)$ . Motivated by the results in Tuckwell (2008) we consider the model in its most general form

$$\begin{aligned} du(t) &= (\Delta u(t) + f(u(t)) - \lambda v(t)) dt + \sigma dW(t), \\ dv(t) &= \varepsilon(u(t) - pv(t) + b) dt \end{aligned} \quad (2)$$

with nonlinearity  $f(u) = \kappa u(1 - u)(u - a)$ ,  $a \in (0, 1)$ ,  $\lambda, \sigma, p > 0$ ,  $\varepsilon \ll 1$  and  $b \in \mathbb{R}$ . Together with initial conditions  $u_0, v_0 \in H$  equation (2) is solvable, as already mentioned above, see (Sauer & Stannat, 2015, Theorem 1). As parameters, we are using the model suggested in Rinzel (1977), also used in Glass & Josephson (1995) to model impulse propagation in cardiac tissue. Set  $a = 0.139$ ,  $\kappa = 1$ ,  $\lambda = 1$ ,  $\varepsilon = 0.008$ ,  $p = 2.54$  and  $b = 0$ . We will always start the system at rest, which is  $(u^*, v^*) = (0, 0)$ . Unless otherwise mentioned, all simulations are done using these values.

For comparison, we also use the parametrization as in Tuckwell (2008), which are essentially the original values by FitzHugh from FitzHugh (1969). These are  $a = 0.5$ ,  $\kappa = 4$ ,  $\lambda = 1$ ,  $\varepsilon = 0.08$ ,  $p = 0.8$  and  $b \approx -0.2979$ . Here, the equilibrium values are  $(u^*, v^*) = (0.1538, -0.1802)$ . Together with a finite rectangular shaped input signal via the Neumann boundary at 0 of the form (1), the solution for both parameter sets has a pulse shape traveling to the right.

## 2.2 Hodgkin-Huxley equations

The Hodgkin-Huxley equations derived from experimental observations squid's giant axon, see Hodgkin & Huxley (1952), are the basis for all subsequent conductance based models for active nerve cells. It describes the evolution of the membrane potential  $u(t, x)$  in time and space by a system of partial differential equations involving the dimensionless potassium activation, sodium activation and sodium inactivation variables  $n(t, x)$ ,  $m(t, x)$  and  $h(t, x)$ , respectively. Adding noise in both variables is physiologically reasonable, see Goldwyn & Shea-Brown (2011), here we focus on the simplest case of current noise. Thus we consider the

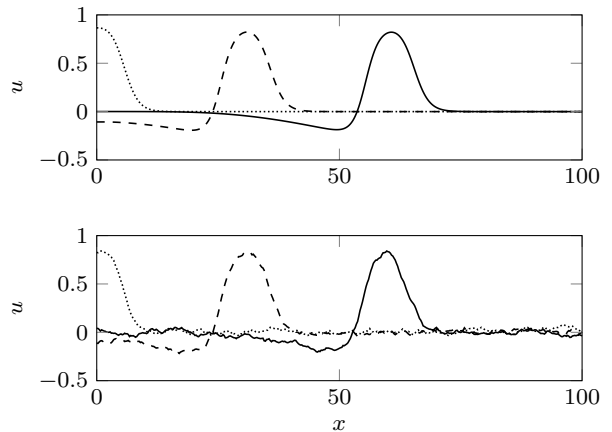


**Fig. 1** The time evolution of  $u$  at  $t_1 = 11$  (dotted),  $t_2 = 86$  (dashed) and  $t_3 = 161$  (solid) for the deterministic pulse ( $\sigma = 0$ ) and one perturbed by noise ( $\sigma = 0.03$ ) on a spatial domain with  $L = 100$  for the first parameter set specified above. Numerical constants can be found in Section 3.

following system

$$\begin{aligned} C_m du(t) &= [a/(2R_i)\Delta u(t) - \bar{g}_K n(t)^4(u(t) - E_K) \\ &\quad - \bar{g}_{Na} m(t)^3 h(t)(u(t) - E_{Na}) \\ &\quad - g_L(u(t) - E_L)] dt + \sigma dW(t), \\ \frac{dn(t)}{dt} &= \alpha_n(u(t))(1 - n(t)) - \beta_n(u(t))n(t), \\ \frac{dm(t)}{dt} &= \alpha_m(u(t))(1 - m(t)) - \beta_m(u(t))m(t), \\ \frac{dh(t)}{dt} &= \alpha_h(u(t))(1 - h(t)) - \beta_h(u(t))h(t). \end{aligned} \quad (3)$$

Here,  $C_m$  is the membrane capacitance in  $\mu\text{F}/\text{cm}^2$ ,  $a$  the axon radius in cm,  $R_i$  the intracellular resistivity in  $\Omega/\text{cm}$ ,  $g_K, g_{Na}, g_L$  the maximal potassium, sodium and leak conductance in  $\text{mS}/\text{cm}^2$ . To further specify units, all times are in ms, voltages in mV and distances in cm. These standard parameters are used throughout:  $a = 0.0238$ ,  $R_i = 34.5$ ,  $C_m = 1$ ,  $g_K = 36$ ,  $g_{Na} = 120$ ,  $g_L = 0.3$ ,  $E_K = -12$ ,  $E_{Na} = 115$  and  $E_L = 10$ . The coefficients determining the evolution of the (in)activation variables are

$$\begin{aligned} \alpha_n(u) &= \frac{10 - u}{100(e^{\frac{10-u}{10}} - 1)}, & \beta_n(u) &= \frac{1}{8}e^{-\frac{u}{80}}, \\ \alpha_m(u) &= \frac{25 - u}{10(e^{\frac{25-u}{10}} - 1)}, & \beta_m(u) &= 4e^{-\frac{u}{18}}, \\ \alpha_h(u) &= \frac{7}{100}e^{-\frac{u}{20}}, & \beta_h(u) &= \frac{1}{e^{\frac{30-u}{10}} + 1}. \end{aligned}$$

As in the case of the FHN equations, we use the equilibrium values  $(u^*, n^*, m^*, h^*)$ , being  $u^* = 0$  and

$$x^* = \frac{\alpha_x(0)}{\alpha_x(0) + \beta_x(0)}, \quad x = n, m, h,$$

as initial values to start the neuron at rest. Note that the membrane potential is shifted by 65mV compared to the original values.

Again, a finite rectangular shaped input signal via the Neumann boundary at 0 of the form (1) yields a solution of pulse shape traveling to the right. Compared to the FHN pulse, this one has a sharper peak and is more localized.

### 2.3 Numerical method

Both SPDEs (2) and (3) are reaction diffusion equations coupled to a set of equations without spatial diffusion. Thus, the main issue from a numerical perspective is the simulation of equations of the form

$$du(t) = \lambda \left( \Delta u(t) + f(u(t)) \right) dt + \sigma dW(t)$$

with Neumann boundary conditions as in (1). The numerical method chosen for the integration of such a SPDE is a finite difference approximation in both space and time, see Sauer & Stannat (2015, 2014) for details. For the space variable  $x$  we use an equidistant grid ( $x_i$ ) of size  $\Delta x = L/N$  and replace the second derivative by its two-sided difference quotient. Boundary conditions are approximated up to second order, using the artificial points  $x_{-1}$  and  $x_{N+1}$ . The time variable  $t$  is discretized to ( $t_j$ ) using  $\Delta t = 1/M$  and a semi-implicit Euler scheme. Approximating the variable  $u$  in the point ( $x_i, t_j$ ) yields the following scheme.

$$\begin{aligned} u_{0,j+1} &= u_{0,j} + \frac{\lambda \Delta t}{\Delta x^2} (2u_{1,j+1} - 2u_{0,j+1}) \\ &\quad + \Delta t f(u_{0,j}) + 2 \frac{\lambda \Delta t}{\Delta x} J_{j+1} + \sigma \sqrt{\frac{\Delta t}{2\Delta x}} N_{0,j}, \\ u_{i,j+1} &= u_{i,j} + \frac{\lambda \Delta t}{\Delta x^2} (u_{i+1,j+1} - 2u_{i,j+1} + u_{i-1,j+1}) \\ &\quad + \Delta t f(u_{i,j}) + \sigma \sqrt{\frac{\Delta t}{\Delta x}} N_{i,j}, \\ u_{N,j+1} &= u_{N,j} + \frac{\lambda \Delta t}{\Delta x^2} (2u_{N-1,j+1} - 2u_{N,j+1}) \\ &\quad + \Delta t f(u_{N,j}) + \sigma \sqrt{\frac{\Delta t}{2\Delta x}} N_{N,j} \end{aligned}$$

for  $1 \leq i \leq N-1$ , where  $J_j$  is the discrete applied current and  $(N_{i,j})_{0 \leq i \leq N, j \geq 1}$  is a sequence of iid  $\mathcal{N}(0,1)$ -distributed random variables. For details on convergence of this scheme and error rates we refer to Sauer & Stannat (2015).

### 3 Reliability of signal transmission

Let us first specify units and numerical parameters. The pulse solution to (2) travels along the axon with a speed of approximately 0.4 space units per time unit. With a space unit being 0.05mm and a time unit being 0.01ms, this equals 2m/s, a number close to the value for unmyelinated axons. Choosing  $L = 100$  yields an axon length of 5mm, which is a realistic setting. The

simulations are done with  $N = 400$ , thus  $\Delta x = 0.25$ ,  $\Delta t = 0.05$ ,  $J = 3$  and  $T^* = 1$ .

Recall the problem concerning how the presence of noise affects the generation and reliability of transmission of action potentials in axons posed in Tuckwell (2008). There appear what we will call *propagation failures* in the following, i. e. the pulse breaks down due to interference with the noise, see Figure 2.

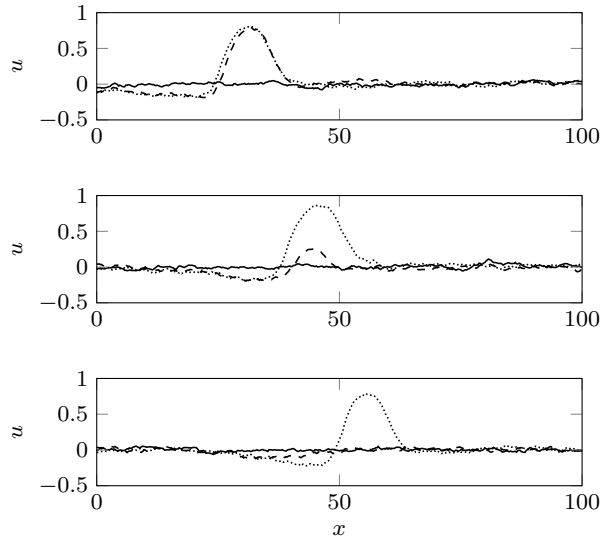


**Fig. 2** A realization of the event *propagation failure* is given by the dashed trajectory. The three plots are the membrane potential  $u$  at times  $t_1 = 91$ ,  $t_2 = 126$ ,  $t_3 = 151$  from top to bottom. For comparison we include a trajectory, where no propagation failure occurs (dotted), and one where the neuron had no input signal and is still fluctuating around the resting potential (solid). For all of them,  $\sigma = 0.03$ .

We aim to propose a simple statistical estimator that allows for detection of a propagation failure. A first educated guess suggests the following functionals of the membrane potential

$$\Phi(u) := \int_0^L u(x) - u^* dx, \quad \tilde{\Phi}(u) := \sup_{x \in (0,L)} u(x) - u^*,$$

describing the area below the pulse of the membrane potential and the maximal pulse height, respectively. Consider the deterministic solutions (i. e.  $\sigma = 0$ )  $\hat{u}$  (pulse) and  $u^*$  (at rest) corresponding to input  $J$  and no input, respectively. Clearly,  $\Phi(\hat{u}) > 0$  and  $\Phi(u^*) = 0$  as well as  $\tilde{\Phi}(\hat{u}) > 0$  and  $\tilde{\Phi}(u^*) = 0$ . Thus, both functionals separate the pulse solution from the resting state. Note that a similar criterion as  $\tilde{\Phi}$  has been used in Faisal & Laughlin (2007) to detect arrival times of action potentials, namely if  $u(t, x) > 1/2\tilde{\Phi}(\hat{u})$  the action potential arrived at spatial position  $x$  at time  $t$ . However, we choose  $\Phi$  over  $\tilde{\Phi}$  for the following reasons. First,  $\Phi$  is linear in

$u$ , whereas  $\tilde{\Phi}$  is nonlinear. Second, conditions on  $\Phi(u)$  form a global criterion, where local fluctuations due to the noise do not have a pronounced effect compared to the local criterion imposed by  $\tilde{\Phi}$ , and third,  $\Phi$  is not sensitive to fluctuations in the phase of the traveling pulse, which will be explained in Section 5.

Now, let us focus on  $\Phi$ . As a visualization, see Figure 3 for the time evolution of  $\Phi(u_j(t))$ ,  $j = 1, 2, 3$ , where  $u_j$  correspond to the same realizations as in Figure 2. One can observe from the graph, that sometime shortly after  $t_1 = 91$  the dashed pulse begins to break down until its area crosses 0 around  $t_2 = 126$ . Note that the pulse is still there, however the after-wave due to recovery is now the bigger contribution.

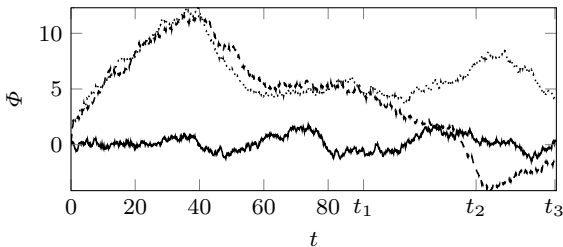


**Fig. 3** The evolution of the area  $\Phi$  for the same realizations as in Figure 2 using the corresponding same line style.

There appears to be a clear distinction between the values of  $\Phi(u)$ , where  $u$  shows no, one or any number of pulses. In order to sustain this argument, let us consider the distribution of  $\Phi(u(T))$  at some appropriate terminal time  $T > 0$ . In this particular example we choose  $T = 200$ . With this choice the pulse likely has yet to reach the right boundary. Note that the speed of propagation itself is, of course, a stochastic process, therefore the arrival times at the boundary fluctuate around the deterministic value. Concerning the distribution, Figure 4 shows a Gaussian kernel density estimate for three different values of  $\sigma$ . For small  $\sigma$  the pulse passes the axon fairly well unchanged and the distribution is concentrated around  $\hat{\Phi} := \Phi(\hat{u}) \approx 5.071$ , which is the value for the deterministic pulse solution  $\hat{u}$ . As  $\sigma$  increases, the shape of the density changes from unimodal to bimodal with a second mode at 0, which represents the propagation failures.

Using the estimator  $\Phi$ , we are able to easily reproduce and generalize the observations made in Tuckwell (2008) in terms of variation of parameters and the number of Monte-Carlo realizations. For a given initialization time  $T_0$ , end time  $T_1$  and suitable critical value  $\theta$  we define the event  $\sup_{t \in [T_0, T_1]} |\Phi(u^\sigma(t)) - \hat{\Phi}| > \theta$  as a *propagation failure* for the noise amplitude  $\sigma$ . Similar,

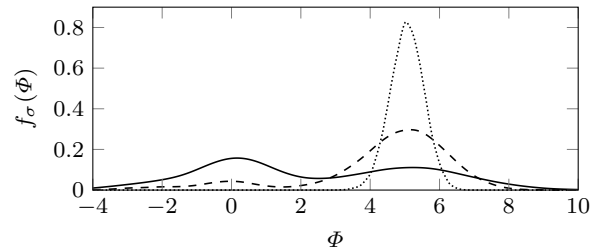


**Fig. 4** A Gaussian kernel density estimate of the density  $f_\sigma(\Phi(u(T)))$  using  $M = 50\,000$  realizations. The values for  $\sigma$  are  $\sigma_1 = 0.014$  (dotted),  $\sigma_2 = 0.032$  (dashed) and  $\sigma_3 = 0.05$  (solid).

the probability of propagation failure is

$$p_\sigma := \mathbb{P} \left[ \sup_{t \in [T_0, T_1]} |\Phi(u^\sigma(t)) - \hat{\Phi}| > \theta \right].$$

Observations of typical realizations suggest  $\theta = 1/2\hat{\Phi}$ ,  $T_0 = 115$  and  $T_1 = 240$ . Figure 5 shows the probability of faithful signal transmission  $1 - p_\sigma$  versus  $\sigma$ .

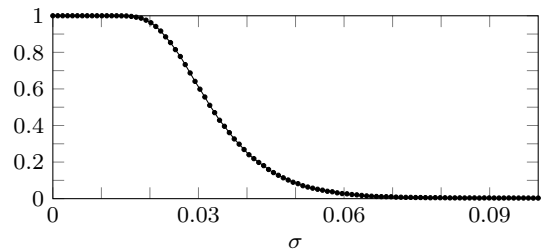


**Fig. 5** Plot of  $1 - p_\sigma$  vs.  $\sigma$  for the FHN equations. Each point represents  $M = 50\,000$  realizations, the resolution for  $\sigma$  is 0.001.

### 3.1 Original FHN parameters

In this section, we use (2) with the parameters from Tuckwell (2008). Again, we can compute an estimate of  $p_\sigma$  based on  $M = 50\,000$  realizations. Comparison with the data from (Tuckwell, 2008, Figure 3) illustrates that our estimator is defective concerning whether or not it can depict the events counted in Tuckwell (2008). The reason is, of course, the dependence on the threshold  $\theta$  that allows variability, in particular a shift of the curve in Figure 5 in a monotone fashion. However, this is the price to pay for a precise definition of a propagation failure in the sense that it discriminates events based on quantitative aspects of the solution. Figure 6 shows a plot of the probability  $1 - p_\sigma$  versus  $\sigma$  for different thresholds in comparison to the data from Tuckwell (2008). It suggests that in this parameter setting,  $\theta = \hat{\Phi}$

is the choice that most accurately resembles the definition/interpretation of Tuckwell.

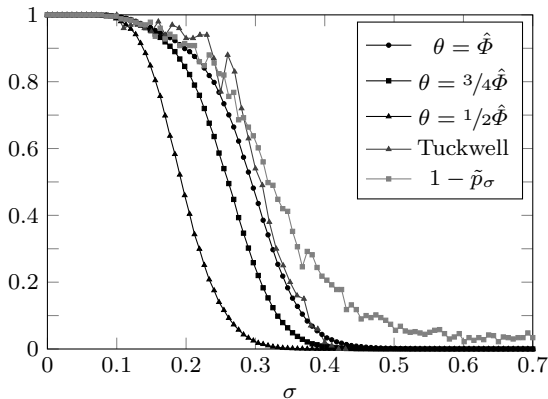


**Fig. 6** Plot of  $1 - p_\sigma$  vs.  $\sigma$  for the FHN equations with the original parameters. Each point represents  $M = 50\,000$  realizations, the resolution for  $\sigma$  is 0.001. Tuckwell's data and  $1 - \tilde{p}_\sigma$  are both based on only 100 realizations for each point.

For comparison, using estimator  $\tilde{\Phi}$  to detect a propagation failure as  $\inf_{t \in [T_0, T_1]} \tilde{\Phi}(u^\sigma(t)) < \tilde{\theta}$ , thus

$$\tilde{p}_\sigma := \mathbb{P} \left[ \inf_{t \in [T_0, T_1]} \tilde{\Phi}(u^\sigma(t)) < \tilde{\theta} \right],$$

leads to the curve  $\sigma \mapsto 1 - \tilde{p}_\sigma$  in Figure 6. Here,  $\tilde{\theta}$  is chosen as one half of the maximal deterministic pulse height. For small  $\sigma$  the estimators  $\Phi$  and  $\tilde{\Phi}$  approximately coincide, but for larger  $\sigma$ , the disadvantages come to light. Large  $\sigma$  leads to large fluctuations and there appear secondary pulses that emerge from these larger fluctuations and later essentially annihilate the original pulse. Thus, such a local criterion may suggest that the pulse is still there, although it already vanished. This underlines our choice in favor of the linear  $\Phi$ .

### 3.2 Hodgkin-Huxley equations

We use the same method to estimate the probability of faithful signal transmission for the standard Hodgkin-Huxley equations as in Section 2.2. With a space unit being 1cm and a time unit being 1ms, the length of the axon is set to  $L = 6$ . Furthermore  $N = 600$ , thus  $\Delta x = 0.01$  and  $\Delta t = 0.05$ . For the input signal we choose  $J = 700$  (in  $\mu\text{A}/\text{cm}^2$ ) and  $T^* = 5$ . The result is shown in Figure 7, using  $M = 10\,000$  realizations,  $\theta = 1/2\hat{\Phi}$ ,  $T_0 = 55$  and  $T_1 = 142.5$ .

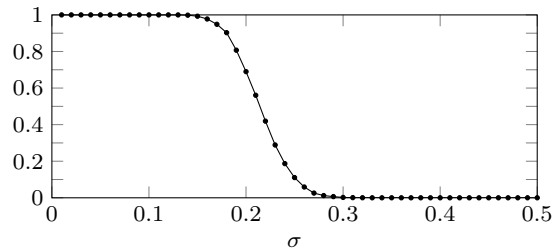


**Fig. 7** Plot of  $1 - p_\sigma$  vs.  $\sigma$  for the Hodgkin-Huxley equations. Each point represents  $M = 10\,000$  realizations, the resolution for  $\sigma$  is 0.01.

## 4 Spontaneous activity

A larger amount of noise applied to (2)/(3) often results in spontaneous disturbances of the resting state that may grow into one or multiple pulses due to the nonlinear dynamics. Depending on the parameter set, the pulse state may be more stable than the resting state, thus this phenomenon becomes more likely than e. g. a propagation failure purely due to noise interference. This is observed in the example using the original FHN parameters and also in the Hodgkin-Huxley case.

Since the estimator  $\Phi$  reliably discriminates between no, one or more pulses, it also can be used to observe the probability of emerging secondary pulses. In this scenario, starting the equations (2)/(3) from their equilibrium point without any input signal through the Neumann boundary condition, we observe the solutions for the time  $T_1$  a pulse would need to reach the right boundary. For a given critical value  $\theta$  we define the event  $\sup_{t \in [0, T_1]} \Phi(u^\sigma(t)) \geq \theta$  as *spontaneous activity* for the noise amplitude  $\sigma$ . Similar, the probability of spontaneous activity is

$$s_\sigma := \mathbb{P} \left[ \sup_{t \in [0, T_1]} \Phi(u^\sigma(t)) \geq \theta \right].$$

In order to be consistent with the observations concerning propagation failures, we choose  $\theta = 1/2\hat{\Phi}$ ,  $T_1 = 240$  and  $M = 50\,000$ . The top plot in Figure 8 shows the probability of spontaneous activity  $s_\sigma$  versus  $\sigma$  in comparison to the probability of propagation failure. One can see that up to  $\sigma = 0.03$  all propagation failures are solely due to interference with the noise with a probability of about  $1/2$ . This is in contrast to the scenario in Tuckwell (2008), where the phenomenon of secondary pulses superposes the propagation failure due to noise interference only.

### 4.1 Hodgkin-Huxley equations

Again, the same method is applied to the Hodgkin-Huxley equations with  $\theta = 1/2\hat{\Phi}$  and  $T_1 = 142.5$ . The

bottom plot in Figure 8 shows the result that differ from the previous section. The graph suggests that all propagation failures are due to spontaneous activity rather than noise interference. This matches the visual inspection of typical realizations, where the pulse remains stable and noise only leads to emerging secondary pulses. Also, note that  $p_\sigma$  is slightly smaller than  $s_\sigma$ , which stems from the fact that the estimator for the event of a propagation failure underestimates the probability due to the frequent occurrence of multiple secondary pulses.

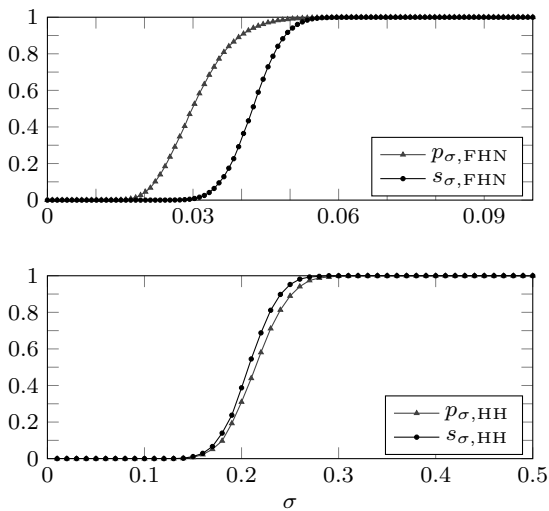


**Fig. 8** Plot of  $s_\sigma$  vs.  $\sigma$  in comparison to the data from Figure 5 (top) and Figure 7 (bottom) using the same parameters.

## 5 Model reduction

Obtaining an analytical expression for  $p_\sigma$  and  $s_\sigma$  is out of reach, considering these are the exit time probabilities of a nonlinear infinite dimensional problem. However, in this part we show that a model reduction is indeed possible and propose a simple, one-dimensional equation that mimics the behavior of the original problem and is able to capture the desired quantities, such as the probabilities of propagation failure and spontaneous activity. This has the following implications: First, the computational costs are reduced and second, we obtain a simplified analytical expression in terms of classical, known quantities. For this reason, consider both (2) and (3) in an abstract form as

$$dX(t) = \left( AX(t) + F(X(t)) \right) dt + \sigma d\mathbb{W}(t), \quad (4)$$

where  $X = (u, v)$  or  $X = (u, n, m, h)$ ,  $A = (\Delta, 0, \dots)^T$ ,  $\mathbb{W} = (W, 0, \dots)^T$  and  $F$  is the appropriate nonlinear

part of the drift. Denote by  $\mathcal{H}$  the product space that is the state space of (4). Let  $\hat{X}$  be the traveling pulse solution and  $X^*$  the resting solution of (4) with  $\sigma = 0$ . For small noise amplitudes, the local behavior of  $Y(t) = X(t) - X^*$  and  $Z(t) = X(t) - \hat{X}(t)$  can be obtained via linearization,

$$dY(t) = [A + \nabla F(X^*)]Y(t) dt + \sigma d\mathbb{W}(t)$$

and

$$dZ(t) = [A + \nabla F(\hat{X}(t))]Z(t) dt + \sigma d\mathbb{W}(t).$$

Here, higher order terms have been neglected. For the remaining part, we assume the following geometrical condition of Lyapunov type

$$\langle [A + \nabla F(X^*)]h, h \rangle_{\mathcal{H}} \leq -\kappa^* \|h\|_{\mathcal{H}}^2, \quad (5)$$

implying that the resting solution is locally exponentially attracting in  $\mathcal{H}$  and

$$\langle [A + \nabla F(\hat{X}(t))]h, h \rangle_{\mathcal{H}} \leq -\hat{\kappa} \|h\|_{\mathcal{H}}^2 + \hat{C} \langle h, d_{\hat{X}}(t) \rangle_{\mathcal{H}}^2, \quad (6)$$

for all  $t \in [T_0, T_1]$ , where  $d_{\hat{X}}(t) = \dot{\hat{X}}(t)$ . Here  $T_0$  is the time until  $\hat{X}$  is in pulse form and  $T_1$  the time it reaches the right boundary. The latter condition can be interpreted geometrically as follows: once it is formed, the traveling pulse solution is locally exponentially attracting in the subspace  $\perp_t := \{h \in \mathcal{H} : \langle h, d_{\hat{X}}(t) \rangle_{\mathcal{H}} = 0\} \subset \mathcal{H}$  that is orthogonal to the direction of propagation. Note that  $\langle \nabla F(\hat{X}(t)), d_{\hat{X}}(t) \rangle_{\mathcal{H}} = \frac{d}{dt} \langle F(\hat{X}(t)), \mathbb{1} \rangle_{\mathcal{H}} = 0$  as well as  $\langle \mathbb{1}, d_{\hat{X}}(t) \rangle_{\mathcal{H}} = \frac{d}{dt} \langle \mathbb{1}, \hat{X}(t) \rangle_{\mathcal{H}} = 0$  for  $t \in [T_0, T_1]$  since the integral is invariant to translation of the pulse.  $\mathbb{1}$  denotes the vector of constant functions equal to 1. Thus,  $\mathbb{1}, \nabla F(\hat{X}(t)) \in \perp_t$  for all  $t \in [T_0, T_1]$ .

**Remark:** Assumption (6) is reasonable, since a similar result has been rigorously proven for the stochastic Nagumo equation and for general stochastic bistable equations in Stannat (2014). It should be possible to extend such results to the systems considered here.

The implications of these stability assumptions are the following. Consider the equation for  $Z(t)$ , that is in particular an Ornstein-Uhlenbeck process on  $\mathcal{H}$ . Writing  $T(t, s) = e^{\int_s^t A + \nabla F(\hat{X}(r)) dr}$ , where the exponential denotes the operator semigroup on  $\mathcal{H}$ , the solution can be written in the mild formulation as

$$Z(t) = T(t, 0)Z(0) + \sigma \int_0^t T(t, s) d\mathbb{W}(s).$$

$Z(t)$  is a Gaussian process, uniquely characterized by its mean and variance

$$\mathbb{E}[Z(t)] = T(t, 0)Z(0),$$

$$\text{Var}[Z(t)] = \sigma^2 \int_0^t T(t, s)T(t, s)^* ds,$$

where  $*$  denotes the adjoint operator. Now, recall  $\Phi(u) = \int_0^L u - u^* dx$ , hence  $\Phi(u(t) - \hat{u}(t)) = \langle u(t) - \hat{u}(t), \mathbb{1} \rangle_H = \langle Z(t), \mathbb{1}_u \rangle_{\mathcal{H}}$ , where  $\mathbb{1}_u = (\mathbb{1}, 0, \dots)^T$ . In particular, this is a linear functional of  $Z(t)$ . Since  $Z$  is Gaussian, so is  $\langle Z(t), \mathbb{1}_u \rangle_{\mathcal{H}}$  with mean and variance

$$\mathbb{E}[\langle Z(t), \mathbb{1}_u \rangle_{\mathcal{H}}] = \langle T(t, 0)Z(0), \mathbb{1}_u \rangle_{\mathcal{H}},$$

$$\text{Var}[\langle Z(t), \mathbb{1}_u \rangle_{\mathcal{H}}] = \sigma^2 \int_0^t \langle T(t, s)T(t, s)^* \mathbb{1}_u, \mathbb{1}_u \rangle_{\mathcal{H}} ds.$$

Now, it is crucial that  $\mathbb{1}_u \in \perp_t$ , i.e. orthogonal to the direction of pulse propagation, and therefore with (6) the semigroup is contracting. In particular it follows that

$$\begin{aligned} \mathbb{E}[\langle Z(t), \mathbb{1}_u \rangle_{\mathcal{H}}] &\leq e^{-\hat{\kappa}t} \|Z(0)\|_{\mathcal{H}} \|\mathbb{1}_u\|_{\mathcal{H}} \\ &\leq \sqrt{L} e^{-\hat{\kappa}t} \|Z(0)\|_{\mathcal{H}}. \end{aligned}$$

Of course, this implies  $\mathbb{E}[\langle Z(t), \mathbb{1}_u \rangle_{\mathcal{H}}] \rightarrow 0$ , which is one of the main advantages of choosing the estimator  $\Phi$ . In contrast to this, the squared  $L^2$ -norm  $\|u(t) - \hat{u}(t)\|_H^2$  or also  $\sup_{x \in (0, L)} |u(t, x) - \hat{u}(t, x)|$  might also serve as a measure of how close  $u$  is to the pulse solution. Both will not converge to 0, since due to the noise  $u$  will never be adapted to the right phase of  $\hat{u}$ . In our approach, we integrate the difference  $u - \hat{u}$  with respect to a function orthogonal to the direction of propagation, hence our estimator does not perceive any phase shift and is locally exponentially stable around 0. Concerning the variance, we compute

$$\begin{aligned} \text{Var}[\langle Z(t), \mathbb{1}_u \rangle_{\mathcal{H}}] &= \sigma^2 \int_0^t \|T(t, s)\mathbb{1}_u\|_{\mathcal{H}}^2 ds \\ &\leq \sigma^2 \int_0^t e^{-2\hat{\kappa}s} ds \|\mathbb{1}_u\|_{\mathcal{H}}^2 \leq \frac{\sigma^2 \sqrt{L}}{2\hat{\kappa}}. \end{aligned}$$

With the considerations above, the following Ansatz for a scalar valued stochastic differential equation for  $\Phi$  is reasonable.

$$d\Phi(u(t) - \hat{u}(t)) = -\alpha\Phi(u(t) - \hat{u}(t)) dt + \tilde{\sigma} d\beta(t),$$

where  $\beta(t) := \sqrt{L}^{-1} \langle W(t), \mathbb{1} \rangle_H$  defines a real-valued Brownian motion and  $\tilde{\sigma} := \sqrt{L}\sigma$ . Using linearity of  $\Phi$ ,  $\hat{\Phi} := \Phi(\hat{u}(t))$  and  $\Phi(t) := \Phi(u(t))$  it follows that

$$d\Phi(t) = \alpha(\hat{\Phi} - \Phi(t)) dt + \tilde{\sigma} d\beta(t), \quad \Phi(0) = \hat{\Phi} \quad (7)$$

is the approximating dynamics, a simple, one-dimensional Ornstein-Uhlenbeck process around the mean  $\hat{\Phi}$ . Also,  $p_\sigma$  can be approximated by the exit time probability

$$\tilde{p}_\sigma := \mathbb{P} \left[ \sup_{t \in [T_0, T_1]} |\Phi^\sigma(t) - \hat{\Phi}| > \theta \right]$$

that is due to symmetry given in terms of a first passage time of the Ornstein-Uhlenbeck process. These are intensively studied in relation to stochastic LIF neurons, see Alili et al. (2005); Sacerdote & Giraudo (2013), and are in addition easily accessible numerically.

In this Ansatz, the whole complexity of the SPDE dynamics is reduced to the parameter  $\alpha$  and the solution to (7) can be written down explicitly as

$$\Phi(t) = \hat{\Phi} + (\Phi(0) - \hat{\Phi})e^{-\alpha t} + \tilde{\sigma} \int_0^t e^{-\alpha(t-s)} d\beta(s).$$

Assuming the validity of this linear approximation, which will be true for small  $\sigma$ , we can estimate  $\alpha$  using mean and variance of  $\Phi(t)$ . In particular,

$$\begin{aligned} \mathbb{E}[\Phi(t)] &= \hat{\Phi} + (\Phi(0) - \hat{\Phi})e^{-\alpha t}, \\ \text{Var}[\Phi(t)] &= \mathbb{E} \left[ \left( \tilde{\sigma} \int_0^t e^{-\alpha(t-s)} d\beta(s) \right)^2 \right] \\ &= \tilde{\sigma}^2 \int_0^t e^{-2\alpha s} ds = \frac{L\sigma^2}{2\alpha} (1 - e^{-2\alpha t}). \end{aligned}$$

Hence,  $\text{Var}[\Phi(t)] \rightarrow L\sigma^2/2\alpha$  as  $t \rightarrow \infty$  can be used to estimate  $\alpha$  for large  $t$ , in our simulations  $t = 240$ , thus the difference to the limit is less than 1%. We apply the standard variance estimator

$$\text{Var}_M := \frac{1}{M-1} \sum_{k=1}^M (\Phi_k(t) - \bar{\Phi}_M)^2, \quad \bar{\Phi}_M := \frac{1}{M} \sum_{k=1}^M \Phi_k(t).$$

In order to further average out errors, we do the estimation for  $\sigma_j = k/100 : k = 1, \dots, 10$ . In the end, this reads as

$$\alpha_M := \sum_{j=1}^{10} \frac{L\sigma^2}{20\text{Var}_M^\sigma} \approx 0.030, \quad (8)$$

with again  $M = 50\,000$  realizations.

Using the linearization around  $X^*$  and the same Ansatz, we propose a similar Ornstein-Uhlenbeck process, whose hitting probabilities approximate  $s_\sigma$ . With  $\Phi(t) := \Phi(u(t)) = \langle u(t) - u^*, \mathbb{1} \rangle_H$  and, of course,  $\Phi(u^*) = 0$  this reads as

$$d\Phi(t) = -\beta\Phi(t) dt + \sigma d\beta(t), \quad \Phi(0) = 0. \quad (9)$$

Also,  $\mathbb{E}[\Phi(t)] = 0$  and  $\text{Var}[\Phi(t)] = L\sigma^2/2\beta(1 - e^{-2\beta t})$  and we estimate the rate  $\beta$  via

$$\beta_M := \sum_{j=1}^{10} \frac{L\sigma^2}{20\text{Var}_M^\sigma} \approx 0.153 \quad (10)$$

with  $M = 50\,000$  realizations. Figure 9 shows the probabilities  $\tilde{p}_\sigma$  and

$$\tilde{s}_\sigma := \mathbb{P} \left[ \sup_{t \in [T_0, T_1]} \Phi^\sigma(t) > \theta \right]$$



as a function of  $\sigma$  for different thresholds  $\theta$  compared to the probabilities obtained using the SPDE. Note that the approximation becomes worse as  $\theta \rightarrow 1$ , which is expected since then the solution approaches the other equilibrium state and the linearization is not valid anymore.

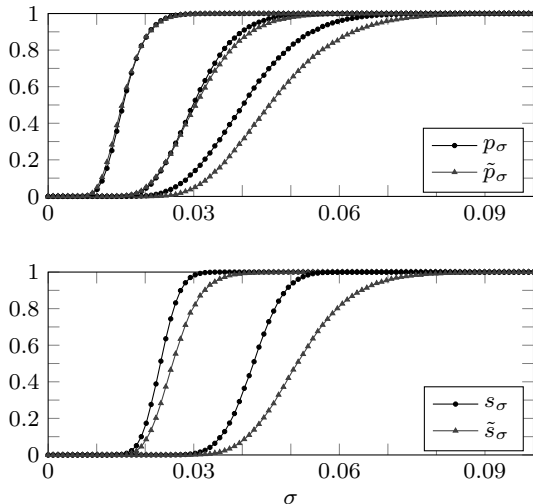


**Fig. 9** Top plot:  $\tilde{p}_\sigma$  vs.  $\sigma$  in comparison to  $p_\sigma$  for the thresholds  $\theta = \{1/4, 1/2, 3/4\}\hat{\Phi}$  from left to right. Bottom plot:  $\tilde{s}_\sigma$  vs.  $\sigma$  in comparison to  $s_\sigma$  for the thresholds  $\theta = \{1/4, 1/2\}\hat{\Phi}$  from left to right. Each point represents  $M = 50\,000$  realizations, the resolution for  $\sigma$  is 0.001.

### 5.1 Comparison with the Hodgkin-Huxley equations

Despite its more complex structure, we apply the same Ansatz to the Hodgkin-Huxley equations for both scenarios. The estimates of the parameters  $\alpha$  and  $\beta$  are  $\alpha_M \approx 0.374$  and  $\beta_M \approx 0.404$ . Figure 10 shows the Ornstein-Uhlenbeck approximation compared to the simulated data from the SPDE.

## 6 Discussion

In this article, we have introduced a method to compute probabilities for spontaneous activity and propagation failure in a consistent way with underlying spatially extended, conductance-based neuronal models, based on certain statistical properties of the membrane potential.

We compared different estimators with respect to the quality of detection, computational costs and robustness and proposed the integral  $\Phi$  of the membrane potential along the spatial domain as an appropriate estimator to detect both spontaneous activity and propagation failure. We discussed the sensitivity of detecting

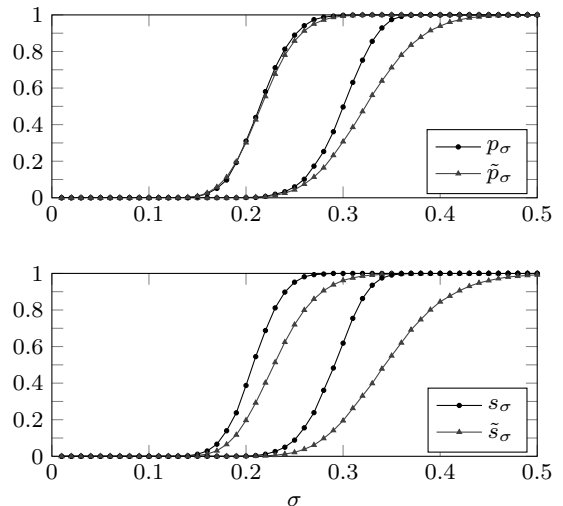


**Fig. 10** Top plot:  $\tilde{p}_\sigma$  vs.  $\sigma$  in comparison to  $p_\sigma$  for the thresholds  $\theta = \{1/2, 3/4\}\hat{\Phi}$  from left to right. Bottom plot:  $\tilde{s}_\sigma$  vs.  $\sigma$  in comparison to  $s_\sigma$  for the thresholds  $\theta = \{1/2, 3/4\}\hat{\Phi}$  from left to right. Each point represents  $M = 50\,000$  realizations, the resolution for  $\sigma$  is 0.01.

propagation failure, depending on the chosen threshold  $\theta$  and presented numerical results for the spatially extended Hodgkin-Huxley and the simpler FitzHugh-Nagumo model.

A further reduction in computational costs and a simplified analytical description can be achieved performing a model reduction with respect to the chosen estimator  $\Phi$  in a consistent way with the underlying spatially extended neuronal model. This is based on its linearization at the resting potential (resp. the traveling action potential) and allows to approximate the probabilities for spontaneous activity and propagation failure in terms of (classical) hitting time probabilities of one-dimensional linear stochastic differential equations. Since the linearization is valid only locally, the approximations  $\tilde{p}_\sigma$  and  $\tilde{s}_\sigma$  become worse for growing  $\theta$  as shown in Figures 9 and 10. For reasonable small  $\theta \leq 1/2\hat{\Phi}$  however, the hitting probabilities of the one-dimensional stochastic differential equations are a solid approximation to the full nonlinear, infinite dimensional SPDE.

As generalizations, we may incorporate more general noise, e. g. as suggested in Goldwyn & Shea-Brown (2011) for the Hodgkin-Huxley model, and study how this affects the signal transmission. Note that the use of channel noise, in form of subunit noise, is in principle possible for the results obtained here and has been done. This does not qualitatively change the behavior concerning  $p_\sigma$  and  $s_\sigma$ , but should be analyzed in comparison to the results in Faisal & Laughlin (2007) for the Hodgkin-Huxley equations with ion channels modeled via Markov chains. However, for such a multiplicative noise the linear Ornstein-Uhlenbeck approximation

that is essentially based on additive noise is not possible anymore in this form.

Future work will also be concerned with the effect of noise on the generation of repetitive spiking, see Tuckwell & Jost (2010), and the estimation of the speed of propagation.

## References

- Alili, L., Patie, P., & Pedersen, J. L. (2005). Representations of the first hitting time density of an ornstein-uhlenbeck process 1. *Stochastic Models*, 21(4), 967–980.
- Faisal, A. A. & Laughlin, S. B. (2007). Stochastic simulations on the reliability of action potential propagation in thin axons. *PLoS computational biology*, 3(5), e79.
- Faisal, A. A., Selen, L. P., & Wolpert, D. M. (2008). Noise in the nervous system. *Nature Reviews Neuroscience*, 9(4), 292–303.
- FitzHugh, R. (1961). Impulses and physiological states in theoretical models of nerve membrane. *Biophysical journal*, 1(6), 445.
- FitzHugh, R. (1969). Mathematical models of excitation and propagation in nerve. In *Biological Engineering*. McGraw-Hill.
- Glass, L. & Josephson, M. E. (1995). Resetting and annihilation of reentrant abnormally rapid heartbeat. *Physical review letters*, 75(10), 2059.
- Goldwyn, J. H. & Shea-Brown, E. (2011). The what and where of adding channel noise to the hodgkin-huxley equations. *PLoS computational biology*, 7(11), e1002247.
- Hodgkin, A. L. & Huxley, A. F. (1952). A quantitative description of membrane current and its application to conduction and excitation in nerve. *The Journal of physiology*, 117(4), 500–544.
- Horikawa, Y. (1991). Noise effects on spike propagation in the stochastic hodgkin-huxley models. *Biological cybernetics*, 66(1), 19–25.
- Nagumo, J., Arimoto, S., & Yoshizawa, S. (1962). An active pulse transmission line simulating nerve axon. *Proceedings of the IRE*, 50(10), 2061–2070.
- Rinzel, J. (1977). Repetitive nerve impulse propagation: numerical results and methods. *Nonlinear Diffusion*, 186–212.
- Sacerdote, L. & Giraudo, M. T. (2013). Stochastic integrate and fire models: a review on mathematical methods and their applications. In *Stochastic Biomathematical Models* (pp. 99–148). Springer.
- Sauer, M. & Stannat, W. (2014). Analysis and approximation of stochastic nerve axon equations. *arXiv preprint arXiv:1402.4791*.
- Sauer, M. & Stannat, W. (2015). Lattice approximation for stochastic reaction diffusion equations with one-sided lipschitz condition. *Mathematics of Computation*, 84(292), 743–766.
- Stannat, W. (2014). Stability of travelling waves in stochastic bistable reaction-diffusion equations. *arXiv preprint arXiv:1404.3853*.
- Tuckwell, H. C. (2008). Analytical and simulation results for the stochastic spatial fitzhugh-nagumo model neuron. *Neural computation*, 20(12), 3003–3033.
- Tuckwell, H. C. & Jost, J. (2010). Weak noise in neurons may powerfully inhibit the generation of repetitive spiking but not its propagation. *PLoS computational biology*, 6(5), e1000794.
- Tuckwell, H. C. & Jost, J. (2011). The effects of various spatial distributions of weak noise on rhythmic spiking. *Journal of computational neuroscience*, 30(2), 361–371.